Site-Selective Cavity Readout and Classical Error Correction of a 5-Bit Atomic Register

Beili Hu,[*] Josiah Sinclair,[*] Edita Bytyqi, Michelle Chong, Alyssa Rudelis, Joshua Ramette, Zachary Vendeiro, and Vladan Vuletić[†]

Department of Physics, MIT-Harvard Center for Ultracold Atoms and Research Laboratory of Electronics, Massachusetts Institute of Technology, Cambridge, Massachusetts 02139, USA

(Received 29 August 2024; revised 24 January 2025; accepted 21 February 2025; published 25 March 2025)

Optical cavities can provide fast and nondestructive readout of individual atomic qubits; however, scaling up to many qubits remains a challenge. Using locally addressed excited-state Stark shifts to tune atoms out of resonance, we realize site-selective hyperfine-state cavity readout across a ten-site array. The state discrimination fidelity is 0.994(1) for one atom and 0.989(2) averaged over the entire array at a survival probability of 0.975(1). To further speed up array readout, we demonstrate adaptive search strategies utilizing global or subset checks. Finally, we demonstrate repeated rounds of classical error correction, showing exponential suppression of logical error and extending logical memory fivefold beyond the single-bit idling lifetime.

DOI: 10.1103/PhysRevLett.134.120801

Neutral-atom arrays are rapidly advancing toward large-scale quantum error correction (QEC). Notable recent demonstrations include 6000-qubit arrays [1], submicrosecond one- and two-qubit gates with fidelities surpassing QEC thresholds [2–6], coherent transport of entangled qubits [7], and operations on 48 logical qubits showing reduction of the logical error rate with code distance [8]. However, neutral-atom QEC experiments to date have been limited to a single round of error correction due to destructive qubit readout [8]. To realize repeated error correction, parallel nondestructive qubit readout [9–11] and continuous reloading [12,13] are being explored. However, the timescales in these demonstrations currently lag behind other operational timescales, limiting logical clock speeds.

Cavity-based state detection is a promising alternative approach for fast and nondestructive readout. Through the Purcell effect [14], a cavity enhances atomic emission into the cavity mode over emission into free space, increasing collection efficiency and enabling atomic-state detection after scattering only a few photons. Making use of this enhancement, multiple experiments have coupled a single atom to an optical cavity and demonstrated fast (tens of microseconds), low-loss ($<1\%$), and high-fidelity ($>99\%$) state detection [15–17]. Scaling up cavity-enhanced readout to many atoms requires interfacing an atom array with a cavity, which has only been recently addressed [18–21]. As an additional challenge to scaling, the cavity couples globally to all atoms inside its mode volume, prohibiting site-resolved readout of multiple atoms. Proposed strategies to scale up cavity readout include shelving atoms in a dark state [9], shifting one qubit level out of resonance [22], or assembling an array of cavities [23–26]. Very recently, cavity measurement of one atom with no observable hyperfine-state decoherence on a second atom outside the cavity mode has been demonstrated in combination with atom transport in 200 μs [17]. However, measuring multiple qubits sequentially potentially forfeits any speedup compared to parallel free-space imaging methods.

In this Letter, we implement a "hiding" strategy for scaling cavity readout to an array of atoms. By locally light-shifting individual atoms on an excited-to-excited-state transition [27–32], we can address any subset of the array on a fast timescale, with minimal effect on the hyperfine ground states. To demonstrate our approach, we sequentially read out an array containing up to ten atoms and show that hidden atoms are well-shielded against probe-induced depumping with only milliwatts of hiding power per atom. To further speed up readout tasks such as syndrome readout for quantum error correction, we implement an "adaptive" search strategy utilizing real-time decision-making, and observe a substantial improvement over deterministic sequential readout. Finally, previewing how cavity readout with real-time feedback can enable repeated rounds of error correction, we implement a classical repetition code, where one bit of information is redundantly encoded in the hyperfine states of an atomic register. We observe exponentially suppressed errors for $d = 3$ and 5 logical bits, and extend the logical bit lifetime fivefold beyond the single-bit idling lifetime, limited mainly by percent-level atom loss.

We load single ^{87}Rb atoms into a one-dimensional array of ten tweezers, located along the axis of an in-vacuum standing-wave optical cavity with a mirror spacing of 4.39 cm and a waist of 45 μm (see Fig. 1). The cavity

[*]These authors contributed equally to this work.

[†]Contact author: vuletic@mit.edu

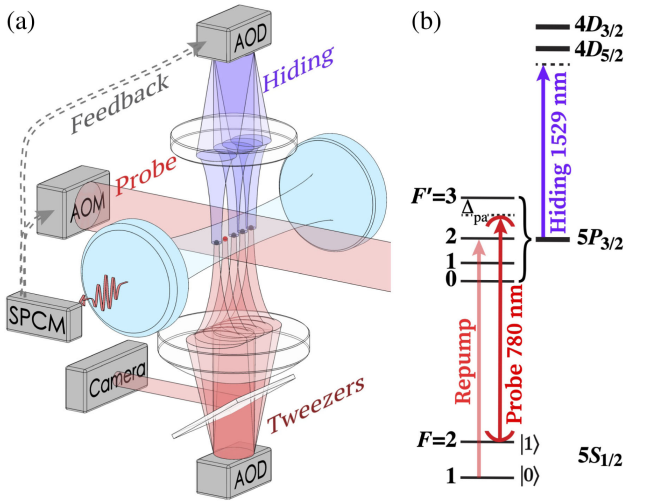

FIG. 1. (a) Experimental setup. Individual atoms are loaded into a one-dimensional tweezer array along the cavity axis, illuminated by a global probe beam switched by an acousto-optical modulator (AOM), and individually addressed hiding beams. Fluorescence is collected from both sides of the cavity (only one side shown) into single-photon counting modules (SPCMs). The probe beam and the hiding beams are controlled in real time by SPCM measurement results. (b) ^{87}Rb level diagram.

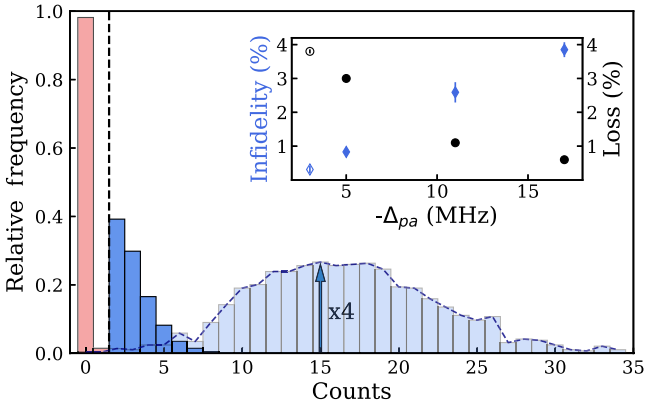

FIG. 2. Hyperfine-state readout ($F = 1, 2$) of a single atom via photon scattering into cavity. Pink, $F = 1$; light blue, $F = 2$ full measurement interval; dark blue, $F = 2$ adaptive measurement. Inset: observed trade-off between atom loss (black circles) and state infidelity (blue diamonds) for an $F = 2$ atom for tweezer depth $U/k_B = 0.25$ mK (solid symbols) and $U/k_B = 0.2$ mK (open symbols).

finesse is $\mathcal{F} = 34000$, giving a maximum cooperativity of $\eta_0 = 4g_0^2/\kappa\Gamma = 2$, with $\{2g_0, \kappa, \Gamma\} = 2\pi \times \{1.1, 0.10, 6.0\}$ MHz, where $2g_0$ is the maximum single-photon Rabi frequency on the ^{87}Rb D_2 cycling transition, and κ and Γ are the decay rates of the cavity and of the atomic excited state, respectively [33]. To encode quantum information in the ground state hyperfine manifolds, we optically pump the atoms with a global depump ($F = 2 \to F' = 2$) or repump ($F = 1 \to F' = 2$) pulse.

We first characterize cavity readout for a single tweezer. The tweezer is illuminated from the side with a pair of counterpropagating probe beams, each with a waist of 0.9 mm and a power of 36 μW, detuned by $\Delta_{pa}/(2\pi) = -5$ MHz below the D_2 $F = 2 \to F' = 3$ transition and in a lin⊥lin configuration for polarization gradient cooling. The cavity resonance frequency is tuned to be $\kappa/2$ above the probe frequency for cavity cooling [34] of the atom. The resulting fluorescence is collected from both sides of the cavity and summed using two single-photon counting modules (SPCMs), with a 27% total efficiency (50% loss at the cavity mirrors, 83% optical path efficiency, and 65% SPCM efficiency). We use a pair of 200 μs-long cavity-enhanced fluorescence measurements to determine tweezer occupation and atomic hyperfine state. In the first measurement interval, the number of collected photons indicates the hyperfine state of the atom, with $F = 2$ being the bright state and $F = 1$ the dark state. In the second interval, we detect atom presence by turning on a repumper beam. The atom is then recooled and optically pumped before the next measurement.

Figure 2 shows a histogram of collected photon counts in the first interval, conditioned on atom presence in the second interval. The bright peak exhibits super-Poissonian statistics due to variations in the atom position relative to the cavity standing wave, which affect the effective cooperativity. The detection threshold is drawn between one and two photons, limited by the 60 s^{-1} combined dark count rate of the two SPCMs. Over a full 200 μs measurement, we collect an average of 15 photons from an $F = 2$ atom (light blue), and much less than one photon from an $F = 1$ atom (pink). However, photons that arrive after the threshold has been surpassed provide no additional information and only contribute to atom heating that results in loss. To suppress this measurement-induced loss, we use a Quantum Machines OPX device to implement an adaptive measurement in all subsequent results, checking the SPCM counts every 20 μs and switching off the probe beams as soon as the threshold is surpassed [35–40]. The resulting photon number distribution (dark blue) is highly non-Poissonian, with a tail coming from multiple photons arriving in the same subinterval. Adaptively terminating the measurement reduces the average number of collected photons by a factor of 5.3(1) and bright-state atom loss by a factor of 4.5(2).

The state-averaged measurement fidelity is 99.4(1)% (see Table I), and is limited by the moderate cavity cooperativity and 5 MHz detuning from the cycling transition, effectively increasing the probability for off-resonant hyperfine-changing scattering events into free space. The measured scattering rate and fidelity agree within 50% with the result of a Jaynes-Cummings Hamiltonian simulation [41], taking into account the spatially averaged cooperativity over nodes and antinodes, a threefold reduction in cavity scattering rate due to mixed

TABLE I. State detection infidelity and loss probability (in %) for cavity readout of a single atom at different tweezer depths U and probe-cavity detunings $-\Delta_{pc}$.

		$F=1$		$F=2$	
U/k_B	$-\Delta_{pc}/2\pi$	Infidelity	Loss	Infidelity	Loss
0.20 mK	3 MHz	0.17(7)	3.0(1)	0.3(1)	3.8(1)
0.25 mK	5 MHz	0.39(7)	2.1(1)	0.8(1)	3.0(1)
0.25 mK	11 MHz	0.30(8)	0.7(1)	2.6(3)	1.1(1)
0.25 mK	17 MHz	0.36(5)	0.3(1)	3.9(2)	0.6(1)

probe polarizations [17], as well as cavity filtering of a Doppler-broadened emission spectrum. Our cavity readout supports a trade-off between loss and bright-state hyperfine fidelity (inset of Fig. 2 and Table I). Choosing a smaller probe-atom detuning suppresses off-resonant, hyperfine-changing scattering events, improving measurement fidelity. However, polarization gradient cooling becomes less effective, resulting in more loss. For atoms in 0.25 mK traps, we estimate an atom temperature of approximately 30 μK at −17 MHz detuning, and 60 μK at −5 MHz detuning using release-and-recapture measurements. We separately observe that atoms in deeper tweezers produce a broadened Doppler emission spectrum, which reduces the effective cavity cooperativity and hence the fidelity. The lowest infidelity is observed with a small probe-cavity detuning and a shallow trap.

We next demonstrate scalable site-selective readout of an atom array coupled to an optical cavity. By applying individually addressed light shifts to excited states, we hide all but the target atom from the probe beam, suppressing scattering and protecting hyperfine information while performing a cavity readout of the target atom. At 1529.420 nm, the light-shifting beam is 7 GHz below the $5P_{3/2} \rightarrow 4D_{5/2}$ transition and 20 GHz below the weaker $5P_{3/2} \rightarrow 4D_{3/2}$ transition, resulting in a polarizability that is about 22 000 times larger for the $5P_{3/2}$ excited state than for the $5S_{1/2}$ ground state [42]. This disparity allows us to rapidly toggle 2 GHz light shifts on the excited state, without jostling atoms in the ground state. Moreover, by choosing to shift nontarget atoms out of resonance, rather than target atoms into resonance, the system is robust to alignment and power drifts.

The light-shifting beams are generated by an acousto-optic deflector (AOD), allowing fast switching on the order of a few μs. By dragging a single atom across a beam and observing the change in scattering rate, we measure a beam waist of 4 μm and a light shift of 1 MHz/μW at the beam center in the low-intensity limit [43]. We observe 1% residual light shift at around 10 μm from the beam center, which we attribute largely to optical aberrations arising from focusing through an aspheric lens at a nondesign wavelength. To avoid crosstalk, atoms are spaced 17 μm apart in all measurements, limiting the array size, but closer spacing of atoms should be possible with an improved optical system.

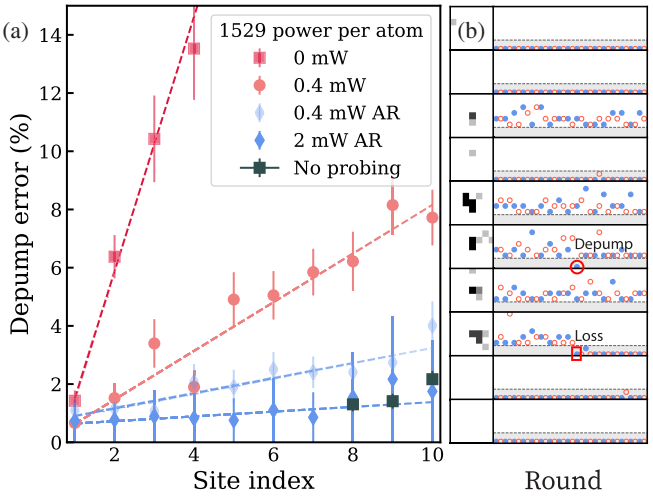

FIG. 3. (a) Bright-state depump errors for sequential cavity readout of up to 10 atoms prepared in $F=2$. AR, adaptive rounds where in every round of sequential measurements, we only measure atoms present in the last round; no probing, depump errors from waiting in the tweezer for 7, 8, and 9 intervals with no probe applied; 0 mW, the same single atom is measured repeatedly to characterize probe-induced depump errors. For all measurements, a tweezer depth of $U/k_B = 0.25$ mK and a probe detuning of 5 MHz were used. For the highest hiding power used, the y intercept is fitted to 0.6(1)% and the slope to 0.08(3)%/site, corresponding to the single-atom state preparation and measurement error and the additional error from scaling, respectively, the latter being dominated by depumping due to idling in 808 nm tweezers. (b) Example single experimental realization. Left: camera image indicating tweezer occupation. Right: collected photon counts from repeated rounds of state preparation in $F=2$ and adaptive cavity readout. In each round, ten tweezers are probed sequentially, alternating between hyperfine (blue solid symbols) and occupation (pink open symbols) measurements. Gray shaded area indicates detection threshold; red circle (rectangle) indicates a bit flip error (atom loss).

Figure 3(a) shows the state preparation and measurement errors in a sequential measurement of 10 sites, using a tweezer depth of $U/k_B = 0.25$ mK, a probe detuning of 5 MHz, and all initialized in the bright state $F=2$. To calibrate how much the hiding beams suppress probe-induced depump errors ($F=2 \rightarrow F=1$) in a sequential measurement, we first separately characterize the depump errors by loading and repeatedly measuring a single atom, finding an increase of 4.4(3)% at the end of each full probe interval. With an intermediate hiding power of 0.4 mW per atom, depump errors are suppressed by a factor of 5.2(6). Depump errors can be even further suppressed using an adaptive strategy where we only measure tweezers that were occupied in the previous round. Combining this adaptive strategy with 2 mW of hiding power per atom

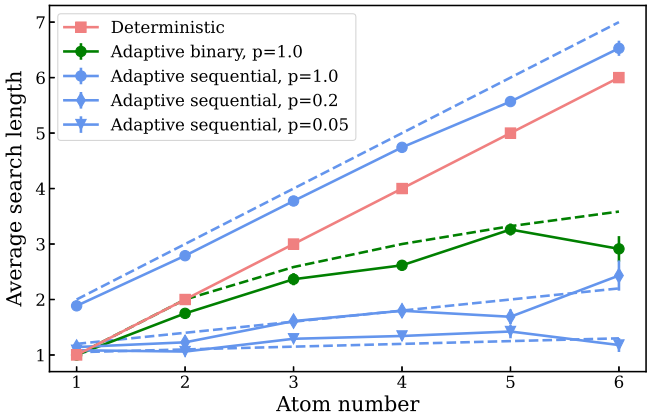

FIG. 4. Average lengths of deterministic and experimentally implemented adaptive search strategies. The adaptive sequential (binary) strategy [blue (green)] consists of a sequential (binary) search conditioned on the result of a global check. The probability that a bright atom is present in an array of N atoms is p. Dashed lines depict $1 + pN$ and $1 + p\log_2 N$. For a deterministic search (red squares) each atom would be checked sequentially, scaling as N.

suppresses the probe-induced depumping sufficiently to be indistinguishable from background depumping from the 808 nm optical tweezer at 0.08(3)% per interval.

When scaling to larger arrays, a sequential readout erodes the cavity's speed advantage. However, if atoms are biased to be in the dark state, faster-than-sequential strategies are available. In this case, it becomes advantageous to unhide and read out groups of atoms at a time, using a single fluorescence interval to reveal if any bright-state atom(s) are present (see [44]). If not, the readout is complete; otherwise, locating the error then resembles a search problem and can be sped up by further partitioning the array. This scenario is relevant to quantum error correction, where all syndrome qubits will be highly biased in a code operating below threshold (typically 1%).

To demonstrate speedup in reading out biased qubits, we prepare a register of N atoms in the dark state $F = 1$, and with probability p pump one atom into the bright state $F = 2$. We implement a simple adaptive strategy: in the event where the global check detects a bright-state atom, we locate it by sequentially reading out the entire register. As shown in Fig. 4, this reduces the average number of cavity readout intervals from N to $1 + pN$ (blue), and it is further reduced to $1 + p\log_2 N$ (green) by partitioning the array and performing a binary search.

As a preparation for future cavity-enabled quantum error correction in an array of atoms with Rydberg interactions [3–8], we implement repeated rounds of classical error correction with a register of atomic bits. As shown in Fig. 5(a), in each experiment, a logical bit $\{0, 1\}$ is encoded in the hyperfine state $F = \{1, 2\}$ of multiple atoms. We introduce bit flip errors on each atom by varying the idling time between state preparation and measurement, with idling errors dominated by background depump or repump from 808 nm tweezers. All atoms are measured sequentially, and a majority vote is taken to determine the logical state. If the majority vote results in a tie, or if no atoms remain, the result is given by a coin toss. Atoms are then reinitialized according to the measurement result, and this cycle of preparation, measurement, and error correction continues for up to 17 rounds.

In Fig. 5(b), we postselect on the number of atoms present in each error-correction round, and extract logical bit error probability for distance $d = 1$, 3, and 5 logical bits given varying physical bit error probabilities. For one atomic bit, the logical error probability equals the physical error probability. We fit the $d = 3$ and 5 data to power laws, finding exponents 2.0(1) and 3.4(3), respectively. The fitted exponents are consistent with $(d + 1)/2$, in agreement with

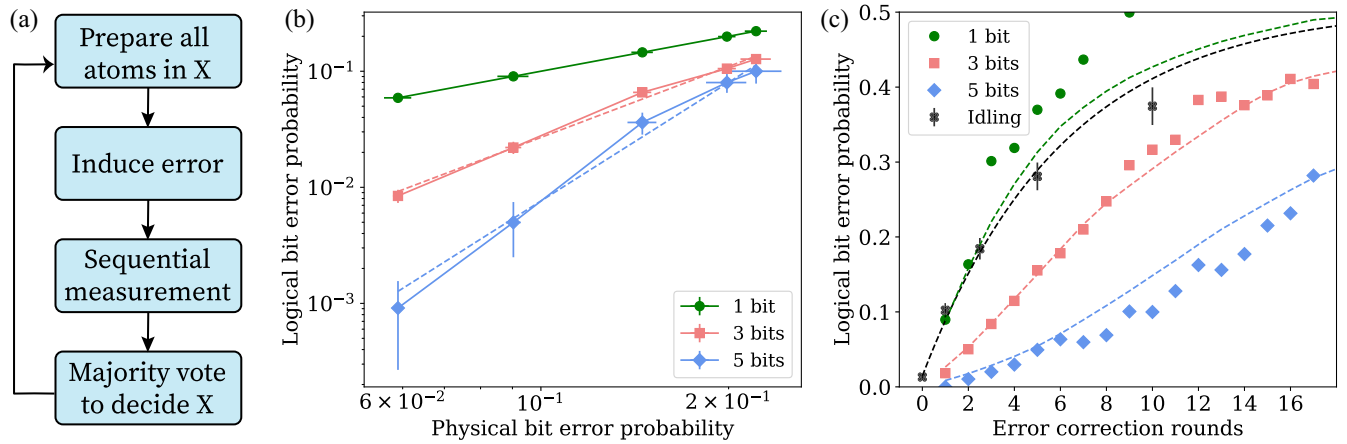

FIG. 5. (a) Experimental flow chart for a classical error correction cycle. (b) Exponential suppression of logical error with increasing code distance. (c) Despite losses, encoding a logical bit in three or five atomic bits results in a decreased chance of an error and increased lifetime compared to an idling atomic bit. Dashed lines are Monte Carlo simulations using single atom error probability (9%) and loss probability (3.7%) extracted from the same dataset.

the expectation of exponential suppression of logical bit error rate with increasing distance d.

In an error-correction scenario with atom loss, measurement-induced or vacuum losses shrink the code distance throughout repeated rounds. Without replenishing the lost atoms, we nonetheless observe in Fig. 5(c) that losses are sufficiently low for a logical bit encoded in three or five physical bits to be preserved beyond the physical-bit idling lifetime. The physical-bit idling lifetime, 125 ms, is a combination of separately measured depump or repump timescale (150 ms) and vacuum lifetime (800 ms). Varying the idling time between rounds, we find that the logical lifetime is maximized with 20 ms of idling, where measurement loss and vacuum loss are balanced. A $d = 1$ logical bit has slightly worse performance than a physical idling bit due to measurement-induced losses and errors. For $d = 3$ and 5 logical bits, we observe a significant reduction in the logical bit error probability, and the logical bit lifetime (defined as the time when error probability reaches $1/e$ of its final value) is extended by a factor of 2.5 and 4.9 compared to the physical-bit idling lifetime.

In summary, we have realized for the first time site-selective hyperfine-state readout of a ten-site ^{87}Rb atom array with an optical cavity. For application to quantum error correction, we have demonstrated the use of adaptive searches to further speed up syndrome readout, and our site-selective cavity readout could be applied with microsecond switching time to any subset of a 1D or 2D array of hundreds of syndrome qubits with commercial lasers. Eventually, we envision using the cavity mode as a readout zone, with batches of syndrome qubits transported in and out, and the coherence of the data qubits protected in a separate storage zone. Combined with state-of-the-art cavities [16,17] capable of 10 μs readout times, our site-selective adaptive approach could enable nondestructive readout of 1000 syndrome qubits containing 0.3% errors in 0.3 ms. Finally, we have demonstrated 17 rounds of real-time classical error correction of a logical bit encoded in an atomic register, marking the first realization of classical repetitive error correction in neutral atoms. When combined with Rydberg quantum gates [3–6] and single-qubit rotations [2], the demonstrated approach will enable repeated rounds of full quantum error correction. For different applications, the site-selective excited-state shift can be used to control atom-cavity coupling for multiplexed entanglement generation [21,45–50] or programmable atom-atom interactions [51–55], and may also prove useful for continuous reloading and midcircuit readout in free space.

Acknowledgments—We gratefully acknowledge Tout Wang and Mikhail D. Lukin for valuable discussions as well as loaning us the 1529 nm laser, Luke Stewart for contributions to the experimental setup, and Ziv Aqua for comments on the manuscript. This project was funded in part by DARPA under the ONISQ program (Grant No. 134371-5113608), the MIT-Harvard Center for Ultracold Atoms (NSF Grant No. PHY-1734011), Quera, and the ARO (Grant No. W911NF1910517). Support is also acknowledged from the U.S. Department of Energy, Office of Science, National Quantum Information Science Research Centers, Quantum Systems Accelerator (Contract No. 7571809).

[1] H. J. Manetsch, G. Nomura, E. Bataille, K. H. Leung, X. Lv, and M. Endres, A tweezer array with 6100 highly coherent atomic qubits, arXiv:2403.12021.

[2] H. Levine, D. Bluvstein, A. Keesling, T. T. Wang, S. Ebadi, G. Semeghini, A. Omran, M. Greiner, V. Vuletić, and M. D. Lukin, Dispersive optical systems for scalable Raman driving of hyperfine qubits, Phys. Rev. A **105**, 032618 (2022).

[3] S. Ma, G. Liu, P. Peng, B. Zhang, S. Jandura, J. Claes, A. P. Burgers, G. Pupillo, S. Puri, and J. D. Thompson, High-fidelity gates and mid-circuit erasure conversion in an atomic qubit, Nature (London) **622**, 279 (2023).

[4] S. J. Evered, D. Bluvstein, M. Kalinowski, S. Ebadi, T. Manovitz, H. Zhou, S. H. Li, A. A. Geim, T. T. Wang, N. Maskara, H. Levine, G. Semeghini, M. Greiner, V. Vuletić, and M. D. Lukin, High-fidelity parallel entangling gates on a neutral-atom quantum computer, Nature (London) **622**, 268 (2023).

[5] R. B.-S. Tsai, X. Sun, A. L. Shaw, R. Finkelstein, and M. Endres, Benchmarking and linear response modeling of high-fidelity Rydberg gates, PRX Quantum **6**, 010331 (2025).

[6] A. G. Radnaev *et al.*, A universal neutral-atom quantum computer with individual optical addressing and non-destructive readout, arXiv:2408.08288.

[7] D. Bluvstein, H. Levine, G. Semeghini, T. T. Wang, S. Ebadi, M. Kalinowski, A. Keesling, N. Maskara, H. Pichler, M. Greiner, V. Vuletić, and M. D. Lukin, A quantum processor based on coherent transport of entangled atom arrays, Nature (London) **604**, 451 (2022).

[8] D. Bluvstein *et al.*, Logical quantum processor based on reconfigurable atom arrays, Nature (London) **626**, 58 (2024).

[9] M. Kwon, M. F. Ebert, T. G. Walker, and M. Saffman, Parallel low-loss measurement of multiple atomic qubits, Phys. Rev. Lett. **119**, 180504 (2017).

[10] M. Martinez-Dorantes, W. Alt, J. Gallego, S. Ghosh, L. Ratschbacher, Y. Völzke, and D. Meschede, Fast non-destructive parallel readout of neutral atom registers in optical potentials, Phys. Rev. Lett. **119**, 180503 (2017).

[11] T.-Y. Wu, A. Kumar, F. Giraldo, and D. S. Weiss, Stern–Gerlach detection of neutral-atom qubits in a state-dependent optical lattice, Nat. Phys. **15**, 538 (2019).

[12] F. Gyger, M. Ammenwerth, R. Tao, H. Timme, S. Snigirev, I. Bloch, and J. Zeiher, Continuous operation of large-scale atom arrays in optical lattices, Phys. Rev. Res. **6**, 033104 (2024).

[13] M. A. Norcia *et al.*, Iterative assembly of ^{171}Yb atom arrays with cavity-enhanced optical lattices, PRX Quantum **5**, 030316 (2024).

[14] E. M. Purcell, Spontaneous emission probabilities at radio frequencies, Phys. Rev. **69**, 674 (1946), https://journals.aps.org/pr/pdf/10.1103/PhysRev.69.674.2.
[15] J. Bochmann, M. Mücke, C. Guhl, S. Ritter, G. Rempe, and D. L. Moehring, Lossless state detection of single neutral atoms, Phys. Rev. Lett. **104**, 203601 (2010).
[16] R. Gehr, J. Volz, G. Dubois, T. Steinmetz, Y. Colombe, B. L. Lev, R. Long, J. Estève, and J. Reichel, Cavity-based single atom preparation and high-fidelity hyperfine state readout, Phys. Rev. Lett. **104**, 203602 (2010).
[17] E. Deist, Y.-H. Lu, J. Ho, M. K. Pasha, J. Zeiher, Z. Yan, and D. M. Stamper-Kurn, Mid-circuit cavity measurement in a neutral atom array, Phys. Rev. Lett. **129**, 203602 (2022).
[18] T. Đorđević, P. Samutpraphoot, P. L. Ocola, H. Bernien, B. Grinkemeyer, I. Dimitrova, V. Vuletić, and M. D. Lukin, Entanglement transport and a nanophotonic interface for atoms in optical tweezers, Science **373**, 1511 (2021).
[19] Z. Yan, J. Ho, Y.-H. Lu, S. J. Masson, A. Asenjo-Garcia, and D. M. Stamper-Kurn, Superradiant and subradiant cavity scattering by atom arrays, Phys. Rev. Lett. **131**, 253603 (2023).
[20] Y. Liu, Z. Wang, P. Yang, Q. Wang, Q. Fan, S. Guan, G. Li, P. Zhang, and T. Zhang, Realization of strong coupling between deterministic single-atom arrays and a high-finesse miniature optical cavity, Phys. Rev. Lett. **130**, 173601 (2023).
[21] L. Hartung, M. Seubert, S. Welte, E. Distante, and G. Rempe, A quantum-network register assembled with optical tweezers in an optical cavity, Science **385**, 179 (2024).
[22] A. Urech, I. H. A. Knottnerus, R. J. C. Spreeuw, and F. Schreck, Narrow-line imaging of single strontium atoms in shallow optical tweezers, Phys. Rev. Res. **4**, 023245 (2022).
[23] M. Trupke, J. Goldwin, B. Darquié, G. Dutier, S. Eriksson, J. Ashmore, and E. A. Hinds, Atom detection and photon production in a scalable, open, optical microcavity, Phys. Rev. Lett. **99**, 063601 (2007).
[24] C. Derntl, M. Schneider, J. Schalko, A. Bittner, J. Schmiedmayer, U. Schmid, and M. Trupke, Arrays of open, independently tunable microcavities, Opt. Express **22**, 22111 (2014).
[25] G. Wachter, S. Kuhn, S. Minniberger, C. Salter, P. Asenbaum, J. Millen, M. Schneider, J. Schalko, U. Schmid, A. Felgner, D. Hüser, M. Arndt, and M. Trupke, Silicon microcavity arrays with open access and a finesse of half a million, Light **8**, 37 (2019).
[26] D. Shadmany, A. Kumar, A. Soper, L. Palm, C. Yin, H. Ando, B. Li, L. Taneja, M. Jaffe, D. Schuster, and J. Simon, Cavity QED in a high NA resonator, Sci. Adv. **11**, eads8171 (2025).
[27] L. W. Clark, N. Schine, C. Baum, N. Jia, and J. Simon, Observation of Laughlin states made of light, Nature (London) **582**, 41 (2020).
[28] P. Scholl, H. J. Williams, G. Bornet, F. Wallner, D. Barredo, L. Henriet, A. Signoles, C. Hainaut, T. Franz, S. Geier, A. Tebben, A. Salzinger, G. Zürn, T. Lahaye, M. Weidemüller, and A. Browaeys, Microwave engineering of programmable XXZ Hamiltonians in arrays of Rydberg atoms, PRX Quantum **3**, 020303 (2022).
[29] A. P. Burgers, S. Ma, S. Saskin, J. Wilson, M. A. Alarcón, C. H. Greene, and J. D. Thompson, Controlling Rydberg excitations using ion-core transitions in alkaline-earth atom-tweezer arrays, PRX Quantum **3**, 020326 (2022).
[30] M. A. Norcia *et al.*, Midcircuit qubit measurement and rearrangement in a ^{171}Yb atomic array, Phys. Rev. X **13**, 041034 (2023).
[31] G. Bornet, G. Emperauger, C. Chen, F. Machado, S. Chern, L. Leclerc, B. Gély, Y. T. Chew, D. Barredo, T. Lahaye, N. Y. Yao, and A. Browaeys, Enhancing a many-body dipolar Rydberg tweezer array with arbitrary local controls, Phys. Rev. Lett. **132**, 263601 (2024).
[32] K. Barnes *et al.*, Assembly and coherent control of a register of nuclear spin qubits, Nat. Commun. **13**, 2779 (2022).
[33] A. Rudelis, A cavity-coupled Rydberg atom array platform for quantum computing, Ph.D. thesis, MIT, 2023.
[34] V. Vuletić, H. W. Chan, and A. T. Black, Three-dimensional cavity Doppler cooling and cavity sideband cooling by coherent scattering, Phys. Rev. A **64**, 033405 (2001).
[35] D. B. Hume, T. Rosenband, and D. J. Wineland, High-fidelity adaptive qubit detection through repetitive quantum nondemolition measurements, Phys. Rev. Lett. **99**, 120502 (2007).
[36] A. H. Myerson, D. J. Szwer, S. C. Webster, D. T. C. Allcock, M. J. Curtis, G. Imreh, J. A. Sherman, D. N. Stacey, A. M. Steane, and D. M. Lucas, High-fidelity readout of trapped-ion qubits, Phys. Rev. Lett. **100**, 200502 (2008).
[37] M. J. Gibbons, C. D. Hamley, C.-Y. Shih, and M. S. Chapman, Nondestructive fluorescent state detection of single neutral atom qubits, Phys. Rev. Lett. **106**, 133002 (2011).
[38] S. L. Todaro, V. B. Verma, K. C. McCormick, D. T. C. Allcock, R. P. Mirin, D. J. Wineland, S. W. Nam, A. C. Wilson, D. Leibfried, and D. H. Slichter, State readout of a trapped ion qubit using a trap-integrated superconducting photon detector, Phys. Rev. Lett. **126**, 010501 (2021).
[39] S. D. Erickson, J. J. Wu, P.-Y. Hou, D. C. Cole, S. Geller, A. Kwiatkowski, S. Glancy, E. Knill, D. H. Slichter, A. C. Wilson, and D. Leibfried, High-fidelity indirect readout of trapped-ion hyperfine qubits, Phys. Rev. Lett. **128**, 160503 (2022).
[40] M. N. H. Chow, B. J. Little, and Y.-Y. Jau, High-fidelity low-loss state detection of alkali-metal atoms in optical tweezer traps, Phys. Rev. A **108**, 032407 (2023).
[41] J. Johansson, P. Nation, and F. Nori, Qutip 2: A Python framework for the dynamics of open quantum systems, Comput. Phys. Commun. **184**, 1234 (2013).
[42] N. Šibalić, J. D. Pritchard, K. J. Weatherill, and C. S. Adams, ARC: An open-source library for calculating properties of alkali Rydberg atoms, Comput. Phys. Commun. **220**, 319 (2017).
[43] E. Deist, J. A. Gerber, Y.-H. Lu, J. Zeiher, and D. M. Stamper-Kurn, Superresolution microscopy of optical fields using tweezer-trapped single atoms, Phys. Rev. Lett. **128**, 083201 (2022).
[44] Note that the single-atom adaptive readout continues to be useful when reading out multiple atoms since the total fluorescence rate scales approximately linearly with the number of bright atoms.
[45] W. Huie, S. G. Menon, H. Bernien, and J. P. Covey, Multiplexed telecommunication-band quantum networking with atom arrays in optical cavities, Phys. Rev. Res. **3**, 043154 (2021).

[46] J. P. Covey, H. Weinfurter, and H. Bernien, Quantum networks with neutral atom processing nodes, npj Quantum Inf. **9**, 90 (2023).
[47] V. Krutyanskiy, M. Galli, V. Krcmarsky, S. Baier, D. A. Fioretto, Y. Pu, A. Mazloom, P. Sekatski, M. Canteri, M. Teller, J. Schupp, J. Bate, M. Meraner, N. Sangouard, B. P. Lanyon, and T. E. Northup, Entanglement of trapped-ion qubits separated by 230 meters, Phys. Rev. Lett. **130**, 050803 (2023).
[48] V. Krutyanskiy, M. Canteri, M. Meraner, V. Krcmarsky, and B. P. Lanyon, Multimode ion-photon entanglement over 101 kilometers, PRX Quantum **5**, 020308 (2024).
[49] M. Cetina, A. Bylinskii, L. Karpa, D. Gangloff, K. M. Beck, Y. Ge, M. Scholz, A. T. Grier, I. Chuang, and V. Vuletić, One-dimensional array of ion chains coupled to an optical cavity, New J. Phys. **15**, 053001 (2013).
[50] J. Sinclair, J. Ramette, B. Grinkemeyer, D. Bluvstein, M. Lukin, and V. Vuletić, Fault-tolerant optical interconnects for neutral-atom arrays, arXiv:2408.08955.
[51] S. Welte, B. Hacker, S. Daiss, S. Ritter, and G. Rempe, Photon-mediated quantum gate between two neutral atoms in an optical cavity, Phys. Rev. X **8**, 011018 (2018).
[52] V. D. Vaidya, Y. Guo, R. M. Kroeze, K. E. Ballantine, A. J. Kollár, J. Keeling, and B. L. Lev, Tunable-range, photon-mediated atomic interactions in multimode cavity QED, Phys. Rev. X **8**, 011002 (2018).
[53] A. Periwal, E. S. Cooper, P. Kunkel, J. F. Wienand, E. J. Davis, and M. Schleier-Smith, Programmable interactions and emergent geometry in an array of atom clouds, Nature (London) **600**, 630 (2021).
[54] J. Ramette, J. Sinclair, Z. Vendeiro, A. Rudelis, M. Cetina, and V. Vuletić, Any-to-any connected cavity-mediated architecture for quantum computing with trapped ions or Rydberg arrays, PRX Quantum **3**, 010344 (2022).
[55] N. Sauerwein, F. Orsi, P. Uhrich, S. Bandyopadhyay, F. Mattiotti, T. Cantat-Moltrecht, G. Pupillo, P. Hauke, and J.-P. Brantut, Engineering random spin models with atoms in a high-finesse cavity, Nat. Phys. **19**, 1128 (2023).

End Matter

Appendix: Comment on scalability and atom loss— Although scaling to larger codes would further extend the logical memory, even percent-level losses would accumulate rapidly, degrading the code distance and ultimately limiting the logical lifetime. This highlights the central importance of replenishing lost atoms. Nondestructive readout reduces but cannot eliminate the necessity of replenishing atoms when performing many rounds of error correction and deep circuits. In our experiment, for example, perpetual operation of a $d = 5$ logical bit would require replenishing atoms at a relaxed rate of 10 Hz, well below what has been experimentally demonstrated [12,13].

Comment on coherence during measurement— We note that while depumping errors are suppressed, in its current implementation the measurement of one atom is not expected to preserve coherence between the hyperfine states for other atoms: since we are probing close to the $F = 2 \rightarrow F' = 3$ transition, the atoms can scatter many photons before they are optically pumped to the $F = 1$ manifold, but any hyperfine coherence will be destroyed upon scattering the first photon. We also note that such decoherence poses no problem for qubits that are to be measured in the Z basis, e.g., in quantum error-correction applications. Furthermore, a coherence-preserving measurement could be implemented by using local, rather than global, detection beams.